

# Elastica-based strain energy functions for soft biological tissue

K. Garikipati, S. Göktepe & C. Miehe

November 4, 2018

## Abstract

Continuum strain energy functions are developed for soft biological tissues that possess long fibrillar components. The treatment is based on the model of an elastica, which is our fine scale model, and is homogenized in a simple fashion to obtain a continuum strain energy function. Notably, we avoid solving the full fourth-order, nonlinear, partial differential equation for the elastica by resorting to other assumptions, kinematic and energetic, on the response of the individual, elastica-like fibrils.

## 1 Background

Currently-used strain energy functions for soft biological tissue have two main origins. Some have been adopted from the rubber elasticity and polymer elasticity literature, and others have functional forms that have been chosen to reproduce the characteristic locking behavior observed in experiments (see Fung, 1993, for a detailed treatment). Among the rubber/polymer elasticity models are micromechanically-derived ones, which mostly incorporate entropic elasticity (see Landau and Lifshitz, 1951, for a discussion). Entropic-elasticity models are suitable for materials in which the uncoiling of long chain molecules under axial force causes a decrease in configurational entropy as fewer configurations become available to the molecule vibrating under its thermal energy (see Ogden, 1997, for detailed treatments of these models). However, it is not clear that the application of entropic elasticity is appropriate for many soft biological tissues such as tendons, ligaments and muscles. As an example, consider the case of tendons, which have a high collagen content. Sun et al. (2002) demonstrated by laser trap experiments that the elasticity of the collagen molecule, which is a triple helix with a diameter of 1.5 nm and a contour length (fully uncoiled length) of approximately 300 nm is well-represented by the worm-like chain model of Kratky and Porod (1949). However, collagen is not restricted to the form of long chain molecules in the tendon. It forms fibrils of around 300 nm diameter, and lengths of the order of 100s of  $\mu\text{m}$ . These are further ordered into fibers that can run the entire length of tendons (the order of cm). The entire hierarchical structure has extensive crosslinking, including a longitudinal staggering of the collagen molecules that leads to a characteristic banded structure on the scale of a fibril, and a “crimp” in the fibers with a wavelength of 10 – 50  $\mu\text{m}$ . (Screen et al., 2003; Provenzano and Vanderby, 2006). Given this ordered, hierarchical structure with extensive crosslinking, one must question the use of entropic elasticity. Due to kinematic constraints imposed by the crosslinking it seems unlikely that the collagen molecules are able to sample many configurations via thermal fluctuations. Similar arguments can be made for ligaments and muscles.

Support for this view may be inferred from the experiments of Woo et al. (1987). Strain-controlled cyclic tension tests of canine medial collateral ligaments at temperatures between 2° C

and 37° C showed that the area of hysteresis loops decreased as the temperature of the experiment increased. The use of strain control, implies that the decrease in hysteresis was associated with a reduction in initial modulus of the stress-strain curve. In a standard viscoelastic solid, the initial modulus is a material property; in particular, it is independent of viscosity, and therefore not subject to mechanisms of relaxation that may be perceived as a decrease in modulus. This series of arguments thus leads to the conclusion that, in these experiments, the initial modulus of the stress-strain response was decreasing with an increase in temperature. This decrease in elasticity with increase in temperature is a signature of energetic elasticity, not entropic elasticity, which makes the initial modulus increase with temperature (see Treloar, 1975).

One reason for the attractiveness of entropic elasticity models is that they reproduce the experimentally-observed response of soft biological tissue in uniaxial tension shown in Figure 14. We draw attention to the characteristics: a prolonged initial regime with low modulus (the “toe” region), followed by a short nonlinear regime with rapidly-increasing modulus (the “heel” region) and a final high modulus region. We will refer to this as the characteristic soft tissue response. However, there are other, non-entropic, models that also reproduce this behavior. It has been typical in the biomechanics literature to use strain energy functions with mathematical forms that are designed solely to possess this characteristic response (see Fung, 1993). This second class of models is, however, limited by the lack of microstructural bases for the corresponding strain energy functions.

This paper is founded on the recognition that the characteristic locking behavior can be modelled by an energetic, i.e. non-entropic, model of elasticity that accounts for the uncoiling of crimped fibrils with increasing tension. In these models, the characteristic soft tissue response is therefore determined by the elastica-like stress-stretch behavior of the individual fibrils. This consideration leads to a micromechanically-derived strain energy function for soft tissue, which, as argued above, has the proper basis in energetic elasticity, rather than entropy effects, which are suppressed due to crosslinking.

The realization that characteristic soft tissue response is modelled by the stress-stretch behavior of an elastica—or approximations of it—is hardly new. Diamant et al. (1972) used a planar model of rigid links joined by elastic hinges, which they related to the elastica, to model their observations of stress-stretch behavior of rat tail tendons. In Dale et al. (1972) four kinematic models of crimped fibers were considered: a planar sinusoidal waveform, a helical shape, a zig-zag waveform with hinged apices and a zig-zag with apices that maintain a constant angle while deforming by bending. The change in profile of these waveforms was studied and compared with experiment. Beskos and Jenkins (1975) modelled mammalian tendon as an incompressible composite with a continuous distribution of inextensible fibers with a helical shape. The assumption of inextensibility dominates the response of this model leading to stress locking in uniaxial tension at a finite stretch. The planar assumption was again adopted by Comninou and Yannas (1976), who modelled single collagen fibers as sinusoidal beams. Using the theory of shear deformable beams with linear constitutive relations for axial stretching and bending, but allowing geometric nonlinearities, they obtained a nonlinear stress-strain response of single fibers and extended it to a composite with uniaxial reinforcement by sinusoidal fibers. In Lanir (1978) a planar model of a beam on an elastic foundation was adopted for the mechanical interaction between collagen (modelled as a beam) and elastin (the elastic foundation). Similar ideas were explored by Kastelic et al. (1980), in whose model crimped collagen fibers were modelled by links that have negligible stiffness until fully extended. The classical theory of elastics was used by Buckley et al. (1980) to treat the deformation of slender filaments, and the model was solved numerically. Basu and Lardner (1985) also studied the stress-stretch response of sinusoidal beams in elastic matrices, although they did not make the

link to fibrous soft tissue. A kinematic chain with finite axial stiffness and torsional springs was used by Stouffer et al. (1985) to represent the uncoiling of crimped fibers, and compared against experiments. More recently, Hurschler et al. (1997) developed a strain energy function for tendon and ligament with seven parameters including microstructural organization to describe the stress-stretch behavior. The authors also derived simplified versions of their model that were used to fit experimentally-determined, nonlinear stress-stretch curves. Finally, Freed and Doebring (2005) returned to the assumption of a helical structure for collagen fibrils, and using Castiglano's theorem, obtained the force-displacement relationship.

In this communication, we present a very general and powerful procedure for developing the strain energy function for soft tissue based on the elastica as a model for slender fibers. To fix ideas, we refer to collagen fibers. In a notable departure from the body of work cited above, we first obtain the fully-nonlinear, fourth-order elliptic partial differential equation for the quasistatic deformation of the extensible elastica. The underlying kinematics are fully nonlinear and the elastica's strain energy is assumed to be given by quadratic functions of curvature and the right Cauchy-Green tensor. The difficulty of obtaining analytic solutions of even simpler versions of the governing partial differential equation has been noted by some of the authors cited above. Furthermore, numerical solutions, while possible, will prove both expensive and cumbersome, since our ultimate aim is a strain energy function for composite soft tissue in which the elastic-like fibers are the reinforcements at a microscopic scale. For this reason we have examined a few distinct assumptions that make it possible to obtain solutions for the force-extension response. These assumptions are related to the kinematic and energetic behavior of the microscopic collagen fibrils. In Section 2 we lay down the fundamental problem of the elastica. The cases of elasticas that are restricted to circular and sinusoidal arcs, and have further constraints of kinematics and energetics imposed upon them, are developed in Sections 3 and 4 respectively. The various models for the deforming elastica are compared against each other and against experiment in Section 5. The extension to macroscopic strain energy density functions, from which the tissue stress-stretch response can be obtained, and a basic discussion on convexity appear in Section 6. Closing remarks are made in Section 7.

## 2 The deforming elastica

Consider the elastica, a curve,  $\Gamma \subset \mathbb{R}^3$  parameterized by its arc length coordinate,  $S$ , in the reference (undeformed) configuration (Figure 1). Points along the curve are identified by position vectors  $\mathbf{X}(S) \in \mathbb{R}^3$ . The tangent at  $S$  is  $\mathbf{T}(S) = d\mathbf{X}/dS$ . Using a Cartesian basis of orthonormal unit vectors  $\{\mathbf{e}_1, \mathbf{e}_2, \mathbf{e}_3\}$  it is clear that  $dX_I/dS$  is a direction cosine, say  $\cos \alpha_I$  where  $I = 1, 2, 3$  and  $\alpha_I$  are the corresponding angles of inclination of  $\mathbf{T}$ . Using the Euclidean norm of a vector,  $\|\mathbf{v}\| = \sqrt{\sum_I v_I^2}$ , it then follows that  $\|\mathbf{T}\| = 1$ . The curvature of  $\Gamma$  is  $\kappa_0 = \|d^2\mathbf{X}/dS^2\|$ . In the deformed configuration,  $\gamma$ , points have position vectors  $\mathbf{x}(S) = \mathbf{X}(S) + \mathbf{u}(S)$ . The tangent vector to  $\Gamma$  is carried to  $\mathbf{t}(S) = d\mathbf{x}/dS$ , and by the chain rule it can be written as

$$\mathbf{t} = \frac{\partial \mathbf{x}}{\partial \mathbf{X}} \frac{d\mathbf{X}}{dS}.$$

Introducing the deformation gradient tensor,  $\mathbf{F} := \partial \mathbf{x} / \partial \mathbf{X}$ , gives  $\mathbf{t} = \mathbf{F} \mathbf{T}$ , from which it follows that  $\|\mathbf{t}\|^2 = \mathbf{T} \cdot \mathbf{C} \mathbf{T}$ , where  $\mathbf{C} = \mathbf{F}^T \mathbf{F}$  is the right Cauchy-Green tensor. The stretch along  $S$  will be denoted by  $\lambda := ds/dS = \|\mathbf{t}\|$ , and satisfies  $\lambda > 0$ . As an aside, note that if the arc length in the deformed configuration, say  $s$ , is used to parametrize  $\mathbf{x}$  as  $\mathbf{x}(s)$ , then the tangent with respect

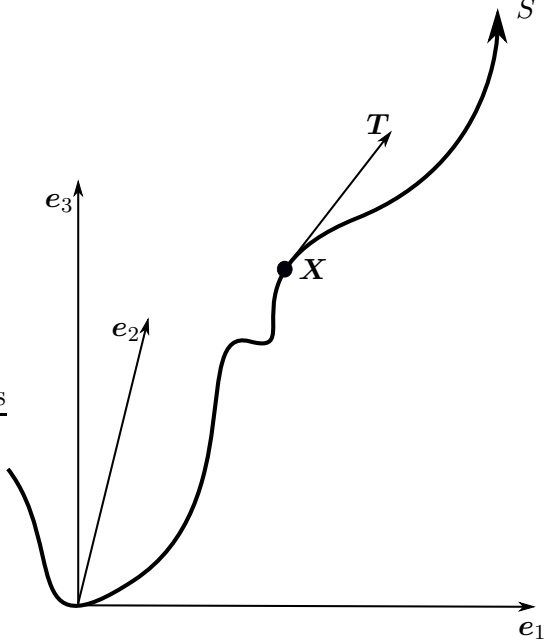


Figure 1: The curve,  $\Gamma \in \mathbb{R}^3$ .

to  $\gamma$ , which we will denote by,  $\mathbf{t}^\#$ , satisfies  $\mathbf{t}^\# = d\mathbf{x}/ds$ , and satisfies  $\|\mathbf{t}^\#\| = 1$ . The curvature of  $\gamma$  is  $\kappa = \|d^2\mathbf{x}/ds^2\|$ , and, clearly, it can be written as  $\kappa = \|d^2\mathbf{x}/\lambda^2 dS^2\|$ .

The strain energy of  $\Gamma$  is assumed to be decomposed into bending and stretching components,  $W(\kappa, \lambda) = K(\kappa) + U(\lambda)$ . The bending stiffness is denoted by  $B$ , the stretching modulus by  $E$ , cross-sectional area by  $A$ , and the reference contour length by  $L$ . This gives

$$K(\kappa) = \int_0^L \frac{1}{2} B(\kappa - \kappa_0)^2 dS, \quad U(\lambda) = \int_0^L \frac{1}{2} EA(\lambda^2 - 1)^2 dS. \quad (1)$$

Observe that  $W(\kappa, \lambda)$ ,  $K(\kappa)$  and  $U(\lambda)$  denote functionals. For simplicity, we will assume that the bending and axial stiffnesses are constant;  $B = \text{const.}$ ,  $EA = \text{const.}$

The governing partial differential equation for the deformation of the elastica is obtained by imposing stationarity of the following free energy functional:

$$\mathcal{G}[\mathbf{u}] = \int_0^L \left( \frac{1}{2} B \left( \left\| \frac{d^2\mathbf{x}}{ds^2} \right\| - \kappa_0(S) \right)^2 + \frac{1}{2} EA \left( \left\| \frac{d\mathbf{x}}{ds} \right\|^2 - 1 \right)^2 - \mathbf{q} \cdot \mathbf{u} \right) dS, \quad (2)$$

where the strain energy has been incorporated from (1) and  $\mathbf{q}(S)$  is the external force per unit contour length. We have also assumed that the displacement is specified at  $S = \{0, L\}$ :  $\mathbf{u}(0) = \mathbf{0}$  and  $\mathbf{u}(L) = \mathbf{g}$ . Introducing the variations  $\mathbf{x}_\varepsilon = \mathbf{X} + \mathbf{u} + \varepsilon \mathbf{w}$ , where  $\varepsilon \in \mathbb{R}$ , and  $\mathbf{w}(S)$  is an arbitrary vector field, satisfying  $\mathbf{w}(S) = \mathbf{0}$  at  $S = \{0, L\}$ , the stationarity condition is

$$\frac{d}{d\varepsilon} \mathcal{G}[\mathbf{u}_\varepsilon] \Big|_{\varepsilon=0} = \frac{d}{d\varepsilon} \left( \int_0^L \left( \frac{1}{2} B \left( \left\| \frac{d^2\mathbf{x}_\varepsilon}{ds^2} \right\| - \kappa_0(S) \right)^2 + \frac{1}{2} EA \left( \left\| \frac{d\mathbf{x}_\varepsilon}{ds} \right\|^2 - 1 \right)^2 - \mathbf{q} \cdot \mathbf{u}_\varepsilon \right) dS \right) \Big|_{\varepsilon=0} = 0. \quad (3)$$

Standard variational calculus, the arbitrariness of  $\mathbf{w}$  and  $d\mathbf{w}/dS$ , as well as the homogeneity of  $\mathbf{w}$  at  $S = \{0, L\}$ , yield the following Euler-Lagrange equations:

$$B \frac{d^2}{\lambda d(\lambda dS)} \left( (1 - \kappa_0/\kappa) \frac{d^2\mathbf{x}}{\lambda d(\lambda dS)} \right) - 2EA \frac{d}{dS} \left( (\lambda^2 - 1) \frac{d\mathbf{x}}{dS} \right) - \mathbf{q} = 0, \quad (4)$$

with the boundary conditions

$$\mathbf{u}(0) = \mathbf{0}, \quad \mathbf{u}(L) = \mathbf{g}, \quad B \left( 1 - \frac{\kappa}{\kappa_0} \right) \frac{d^2\mathbf{x}}{\lambda d(\lambda dS)} = 0 \text{ at } S = \{0, L\}. \quad (5)$$

Since  $\lambda = \|d\mathbf{x}/dS\|$  and  $\kappa = \|d^2\mathbf{x}/\lambda^2 dS^2\|$ , it follows that (4) possesses complexity beyond what is apparent in its form above. In addition to the boundary conditions on  $\mathbf{u}$  at  $\{0, L\}$ , note that the generalized force satisfies homogeneous boundary conditions at  $S = \{0, L\}$  in (5)<sub>2</sub>.<sup>1</sup> Alternate boundary conditions can be used in the above variational procedure.

The ultimate aim of this work is the development of a macroscopic strain energy function, where the micromechanics arises from the deformation of the elastica. The *exact* micromechanics of the deforming elastica is obtained by solving the partial differential equation (4) subject to the boundary conditions in (5). Its solution, however, is nontrivial on account of the nonlinearity and fourth-order form of the partial differential equation. It is therefore desirable to avoid the complexity and expense of solving this equation repeatedly in computations that will use the strain energy function at each material point on the macroscopic scale. For this reason, we examine certain assumptions, kinematic and energetic, which simplify the micromechanics. In Section 3 we make the kinematic assumption that the elastica is constrained to remain the arc of a circle. In Section 4 the deforming elastica is constrained to maintain a sinusoidal waveform.

### 3 Force-displacement response of an elastica constrained to the arc of a circle

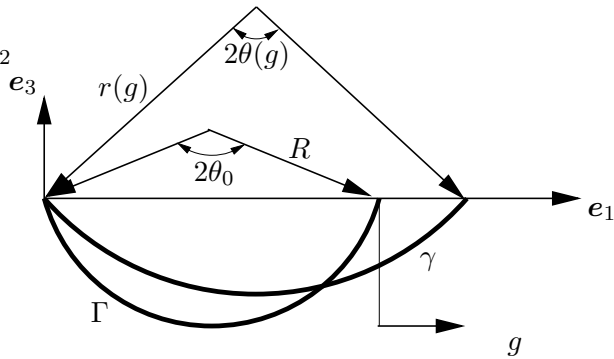


Figure 2: Uncoiling of an elastica shaped as a circular arc.

<sup>1</sup>This generalized force is conjugate to  $d\mathbf{w}/dS$  in the Euler-Lagrange equations arising from (3), and therefore admits the interpretation of a moment.

Consider an elastica with reference configuration,  $\Gamma$ , in the form of an arc of a circle with central angle  $2\theta_0$  and radius  $R$ , as shown in Figure 2. The reference positions of points on  $\Gamma$  are

$$\mathbf{X}(S) = \begin{Bmatrix} R(\sin \theta_0 - \sin(\theta_0 - S/R)) \\ 0 \\ R(\cos \theta_0 - \cos(\theta_0 - S/R)) \end{Bmatrix}, \quad S \in [0, 2R\theta_0] \quad (6)$$

In Sections 3.1–3.3 we explore the effect of further constraints on this deforming elastica. These are the constraints of (i) inextensibility, (ii) incompressibility of the bounding medium, and (iii) stationarity of the energy. The implications of each of these constraints, is discussed further in remarks appearing at the end of the corresponding section. The constraints considered here are not exhaustive. However, the physical interpretations and motivations are transparent.

### 3.1 The inextensible elastica constrained to a circular arc

Let the point  $S = 2\theta_0 R$  be displaced by the vector  $g\mathbf{e}_1$  while the deformed configuration,  $\gamma$  maintains the form of a circular arc without extension, i.e.,  $\lambda = 1$ . Then the tip displacement is restricted to  $0 \leq g \leq 2(\theta_0 - \sin \theta_0)R$ . At a given tip displacement,  $g$ , the central angle of the deformed elastica is  $\theta(g) = \theta_0 R/r(g)$  as depicted in Figure 2. The deformed radius,  $r(g)$ , then satisfies the implicit relation

$$r(g) \sin\left(\frac{\theta_0 R}{r(g)}\right) = R \sin \theta_0 + \frac{g}{2} \quad (7)$$

and the positions of points on  $\gamma$  are

$$\mathbf{x}(S) = \begin{Bmatrix} r\left(\theta - \sin\left(\theta - \frac{S}{r}\right)\right) \\ 0 \\ r\left(\cos \theta - \cos\left(\theta - \frac{S}{r}\right)\right) \end{Bmatrix}. \quad (8)$$

From (6) and (8),

$$\frac{d^2 \mathbf{X}}{dS^2} = \begin{Bmatrix} \frac{1}{R} \cos\left(\frac{S}{R}\right) \\ 0 \\ \frac{1}{R} \sin\left(\frac{S}{R}\right) \end{Bmatrix}, \quad \frac{d\mathbf{x}}{dS} = \begin{Bmatrix} \cos\left(\theta - \frac{S}{r}\right) \\ 0 \\ -\sin\left(\theta - \frac{S}{r}\right) \end{Bmatrix}, \quad \frac{d^2 \mathbf{x}}{dS^2} = \begin{Bmatrix} \frac{1}{r} \sin\left(\theta - \frac{S}{r}\right) \\ 0 \\ \frac{1}{r} \cos\left(\theta - \frac{S}{r}\right) \end{Bmatrix}, \quad (9)$$

from which it follows that  $\kappa_0 = 1/R$ ,  $\kappa = 1/r$  and  $\lambda = 1$ . Note that, for brevity, the dependencies  $r(g)$  and  $\theta(g)$  have been suppressed in both (8) and (9), and for  $g = 2(\theta_0 - \sin \theta_0)R$ ,  $\gamma$  is a straight segment of length  $2\theta_0 R$  along  $\mathbf{e}_1$ . The strain energy of the elastica can now be written, following (1) as

$$W(\kappa; g) = \int_0^{2\theta_0 R} \frac{1}{2} B (\kappa(g) - \kappa_0)^2 dS, \quad 0 \leq g \leq 2(\theta_0 - \sin \theta_0)R \quad (10)$$

Note that in addition to  $W(\kappa; g)$  being a functional of the field,  $\kappa$ , it is a function of the tip displacement,  $g$ . The force response of the elastica to the tip displacement,  $g$ , is

$$f(\kappa; g) = \frac{dW}{dg}, \quad 0 \leq g \leq 2(\theta_0 - \sin \theta_0)R \quad (11)$$

Like  $W$ , the force,  $f$  is a functional of  $\kappa$  and a function of  $g$ . In what follows, the functional character of  $f$  is suppressed since its dependence on  $g$  is of primary interest. Using  $\kappa = \|d\mathbf{x}/ds\|$ , and equations (9), (7) and (10) we have,

$$f(g) = \frac{B\theta_0 R}{r(g)^2} \left( \frac{1}{r(g)} - \frac{1}{R} \right) \frac{1}{\theta \cos \theta - \sin \theta}, \quad 0 \leq g \leq 2(\theta_0 - \sin \theta_0)R. \quad (12)$$

Equation (12) indicates that  $f(g)$  diverges as  $1/r(g) \rightarrow 0$ . Thus the force in a fully uncoiled, inextensible elastica diverges. An extensible elastica, however, develops finite axial tension due to stretching along the tangent as it is uncoiled, and will be considered in the next two sections.

**Remark 1.** The above approach does not involve a formal solution of (4). Instead, it is assumed, *a priori*, that this governing equation is satisfied with the inextensible elastica maintaining the circular arc form. The force conjugate to tip displacement  $g$  has been obtained under these constraints. It is clear that inextensibility is a constitutive restriction here. However, the assumed kinematics, i.e., persistence of the circular arc form can be ensured with a suitable distribution of the force,  $\mathbf{q}(S)$ , which was introduced in (4). We need not concern ourselves with the functional form of this force since it is the tip force alone that is of interest. The assumed strong enforcement of the circular form also makes the deformed shape symmetric about the midpoint of the arc,  $S = \theta_0 R$ . Due to this symmetry the force component  $\mathbf{q} \cdot \mathbf{e}_1$  is *antisymmetric* about  $\theta = \theta_0 R/2r$  and does not contribute to the resultant force along  $\mathbf{e}_1$ . It is this strong assumption of symmetry that allows the force  $f(g)$  to be obtained without explicit solution of (4).

### 3.2 The extensible elastica constrained to a circular arc and subject to a macroscopic incompressibility constraint

Collagen fibrils in soft tissues are surrounded by proteoglycan molecules that bind water. At the levels of stress that the tissue is subject to, the proteoglycan matrix is nearly incompressible. Motivated thus, we consider the deforming fibril constrained to lie within a circumscribing cylinder. The model of an elastica deforming as the arc of a circle in the  $\{\mathbf{e}_1, \mathbf{e}_3\}$  plane is supplemented by requiring invariance of the area of a circumscribing rectangle, even as the rectangle's aspect ratio varies with tip displacement,  $g$ . See Figure 3. The conservation of the area, then, leads us to a closed-form expression for the height,  $a$ , of the current rectangle

$$A_0 \equiv A \quad \leadsto \quad a(g) = \frac{2R^2 \sin \theta_0 (1 - \cos \theta_0)}{2R \sin \theta_0 + g}. \quad (13)$$

Having the explicit form of  $a(g)$ , the radius of the deforming elastica can be readily determined from the geometry of Figure 3 as  $r^2 = (r - a)^2 + (R \sin \theta_0 + g/2)^2$ . This yields

$$r(g) = \frac{1}{2a} \left( (a(g))^2 + \frac{(R^2 \sin \theta_0 (1 - \cos \theta_0))^2}{(a(g))^2} \right). \quad (14)$$

The current curvature  $\kappa(g)$  and stretch  $\lambda(g)$  of the circular elastica then immediately follow as

$$\kappa(g) = \frac{1}{r(g)} \quad \text{and} \quad \lambda(g) = \frac{r(g)\theta(g)}{R\theta_0} \quad (15)$$

where the implicit relation (7) is now replaced by

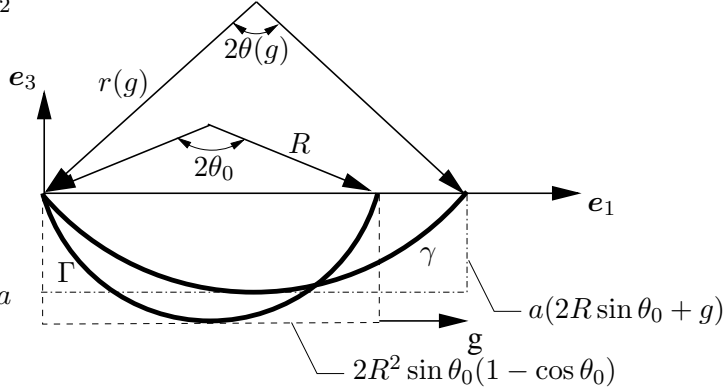


Figure 3: A circular elastica surrounded by an incompressible medium.

$$\theta(g) = \sin^{-1} \left( \frac{R \sin \theta_0 + g/2}{r(g)} \right). \quad (16)$$

See Figure 3. The inextensibility constraint now does not hold:  $\lambda(g) \neq 1$ . Using (15) for  $\kappa(g)$  and  $\lambda(g)$ , and noting that  $\theta$  is a function of  $r(g)$  and  $g$ , we parametrize the strain energy as

$$\overline{W}(r; g) = \int_0^{2\theta_0 R} \frac{1}{2} B \left( \frac{1}{r(g)} - \frac{1}{R} \right)^2 dS + \int_0^{2\theta_0 R} \frac{1}{2} EA \left( \left( \frac{r(g)\theta(g)}{R\theta_0} \right)^2 - 1 \right)^2 dS, \quad (17)$$

where, as previously,  $\overline{W}$  is a functional of  $r$  and a function of  $g$ . The tip force,  $f(g) = d\overline{W}/dg$ , is

$$\begin{aligned} f(g) &= \theta_0 BR \left( \frac{1}{r} - \frac{1}{R} \right) \left( -\frac{1}{r^2} \right) \left( \frac{3R^2 \sin \theta_0 (1 - \cos \theta_0)}{2a^2} - \frac{a^2}{2R^2 \sin \theta_0 (1 - \cos \theta_0)} \right) \\ &+ EA\lambda(\lambda^2 - 1) \left( \frac{1}{\cos \theta} + 2(\theta - \tan \theta) \left( \frac{3R^2 \sin \theta_0 (1 - \cos \theta_0)}{2a^2} - \frac{a^2}{2R^2 \sin \theta_0 (1 - \cos \theta_0)} \right) \right), \end{aligned} \quad (18)$$

where the derivative formulas  $dr/dg = 3R^2 \sin \theta_0 (1 - \cos \theta_0) / 4a^2 - a^2 / 4R^2 \sin \theta_0 (1 - \cos \theta_0)$ ,  $d\theta/dg = \sec \theta / 2r - \tan \theta dr/dg$  and  $d\lambda/dg = (\sec \theta + 2(\theta - \tan \theta)dr/dg) / (2\theta_0 R)$  have been incorporated.

**Remark 2.** Note that the stretch,  $\lambda$ , defined in (15)<sub>2</sub> is averaged over the reference contour length. Its use in the constitutive relation (17)<sub>2</sub> implies that the axial stiffness,  $EA$ , is homogenized over the circular arc with central angle  $2\theta_0$ .

**Remark 3.** For this case of the circular arc-shaped elastica in an incompressible medium, it is found that  $\lambda < 1$  for a certain range of *macroscopic stretch*,  $\bar{\lambda} = 1 + g/2R\sin\theta_0$  (see Section 5.1). The incompressibility constraint causes compression of the elastica. If (4) were solved with this macroscopic incompressibility constraint it would manifest itself as buckling. We have not attempted to follow this one case among the possible states of deformation of the elastica. Instead we have solved for the value of  $\theta_0 = \theta_{0\text{cr}}$  such that for all  $\theta_0 < \theta_{0\text{cr}}$  we have  $d\lambda/d\bar{\lambda} > 0$ , ensuring that macroscopic stretch translates to microscopic stretch. This root is  $\theta_{0\text{cr}} \approx 1.342$ . Our investigation of the circular arc-shaped elastica in an incompressible medium is restricted to  $\theta_0 > \theta_{0\text{cr}}$ .

### 3.3 The extensible elastica constrained to a circular arc, and relaxing to a stationary energy configuration

Referring to Figure 2, and persisting with the stretch,  $\lambda(g)$ , averaged over the reference contour length as in  $(15)_2$ , the central angle,  $\theta(g)$ , of the deformed elastica as in  $(16)$  and  $\kappa(g) = 1/r(g)$  the strain energy is given by  $(17)$ .

For a given tip displacement,  $g$ , corresponding to an applied force,  $f$ , the constraint that the deformed configuration remains the arc of a circle is now supplemented by the requirement that the deformed radius,  $r(g)$ , corresponds to a stationary state of the strain energy of the elastica. The radius,  $r(g)$ , is the solution of the following stationarity condition:

$$\frac{\partial \bar{W}}{\partial r} = 2\theta_0 BR \left( \frac{1}{R} - \frac{1}{r} \right) \frac{1}{r^2} + 4EA\lambda(\lambda^2 - 1)(\theta - \tan \theta) = 0. \quad (19)$$

With the deformed radius thus known, the force is

$$f = \frac{\partial \bar{W}}{\partial g} = 2EA\lambda(\lambda^2 - 1) \sec \theta. \quad (20)$$

Note that the extension of the above results  $(12)$ ,  $(18)$  and  $(20)$  for half-wavelengths to an elastica whose waveform consists of  $n$  such half-wavelengths is straightforward. By symmetry, the force,  $f$ , that results in a total tip displacement of  $g$  corresponds to an extension of  $g/n$  of each half-wavelength, and is obtained from  $(12)$ ,  $(18)$  or  $(20)$  by substituting  $g$  with  $g/n$ .

**Remark 4** Remark 1 on the force field,  $\mathbf{q}(S)$ , that is required to maintain the circular arc-shape also applies here. The assumption of a stationary energy state is perhaps the most compelling of the three cases considered above, implying as it does that the fibrillar structure attains an equilibrium configuration.

## 4 The force-displacement response of a sinusoidal elastica

For the sinusoidal waveform, the reference configuration of the elastica is defined by two shape parameters, the amplitude  $a_0$  and the half-wave length  $l_0$ , see Figure 4. As in Section 3 the elastica

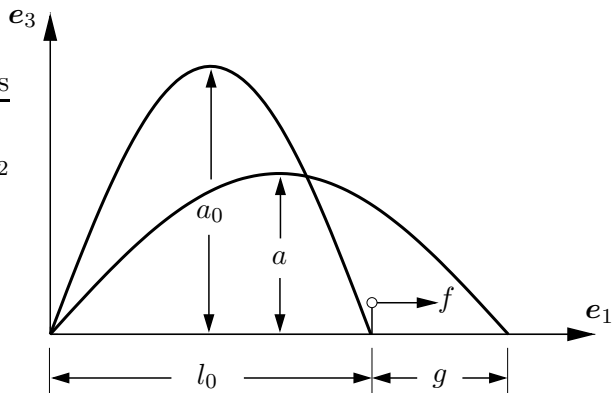


Figure 4: Uncoiling of a sinusoidal elastica.

is constrained to the  $\{e_1, e_3\}$  plane. The reference coordinates of the points on the elastica can be expressed by a single parameter,  $t$ , as

$$\mathbf{X}(t) = \begin{Bmatrix} X_1(t) \\ 0 \\ X_3(t) \end{Bmatrix} = \begin{Bmatrix} t \\ 0 \\ a_0 \sin\left(\frac{\pi}{l_0}t\right) \end{Bmatrix} \quad (21)$$

where  $t \in [0, l_0]$ . Analogously, the shape of a deformed elastica can also be formulated in terms of another spatial parameter,  $\tilde{t}$ ,

$$\mathbf{x}(\tilde{t}) = \begin{Bmatrix} x_1(\tilde{t}) \\ 0 \\ x_3(\tilde{t}) \end{Bmatrix} = \begin{Bmatrix} \tilde{t} \\ 0 \\ a \sin\left(\frac{\pi}{l}\tilde{t}\right) \end{Bmatrix} \quad (22)$$

where all  $\tilde{t} \in [0, l]$ . The value of the current half-wavelength  $l$  is determined by the tip displacement  $g$  through the relation  $l := l_0 + g$ . This definition immediately implies a linear relation between the Eulerian  $\tilde{t}$  and Lagrangian  $t$  parameters

$$\tilde{t} := t l / l_0 = t (1 + g / l_0) \quad \text{and} \quad \partial_t \tilde{t} = l / l_0 = (1 + g / l_0). \quad (23)$$

With this relation at hand, we can further deduce that the argument of the sine functions appearing in both (21) and (22) have the same value, i.e.

$$\alpha(t) := \frac{\pi}{l_0}t = \frac{\pi}{l}\tilde{t}. \quad (24)$$

This geometrical description of the problem allows us to introduce the two main kinematic variables, namely the curvature,  $\kappa$ , and the stretch,  $\lambda$ , as functions of derivatives of  $X_3$  and  $x_3$  with respect to the Lagrangian  $t$  and the Eulerian  $\tilde{t}$  parameters, respectively. For the planar reference and current curves parameterized by the parameters  $t$  and  $\tilde{t}$ , the general curvature formulas given in Section 2 can be simplified to the forms

$$\kappa_0(t) := \frac{X_3''}{(1 + X_3'^2)^{3/2}}, \quad \kappa(\tilde{t}) := \frac{x_3''}{(1 + x_3'^2)^{3/2}}. \quad (25)$$

The superscript  $(\cdot)'$  in (25) denotes the derivatives

$$\begin{aligned} X_3' &:= \frac{\partial X_3}{\partial t} = a_0 \frac{\pi}{l_0} \cos(\alpha(t)), & X_3'' &:= \frac{\partial^2 X_3}{\partial t^2} = -a_0 \frac{\pi^2}{l_0^2} \sin(\alpha(t)), \\ x_3' &:= \frac{\partial x_3}{\partial t} = a \frac{\pi}{l} \cos(\alpha(t)), & x_3'' &:= \frac{\partial^2 x_3}{\partial t^2} = -a \frac{\pi^2}{l^2} \sin(\alpha(t)). \end{aligned} \quad (26)$$

In this framework, the local value of stretch can be calculated by  $\lambda := ds/dS$  where the infinitesimal arc length measures  $dS$ , and  $ds$  are defined by  $dS := \sqrt{dX_1^2 + dX_3^2} = \sqrt{1 + X_3'^2} dt$  and  $ds := \sqrt{dx_1^2 + dx_3^2} = \sqrt{1 + x_3'^2} d\tilde{t}$ , respectively. Then, combining these results with the one given in (23)<sub>2</sub> yields the stretch expression

$$\lambda := ds/dS = \frac{\sqrt{1 + x_3'^2} l}{\sqrt{1 + X_3'^2} l_0}. \quad (27)$$

The basic kinematic variables  $\kappa_0, \kappa(t, g, a(g))$  and  $\lambda(t, g, a(g))$  are thus defined. Note that  $\kappa$  and  $\lambda$  vary pointwise with  $t$  and are parametrized by  $g$  and  $a(g)$ . The total energy of the sinusoidal elastica in the reference configuration is specified to be

$$\widetilde{W}(\kappa, \lambda; g, a(g)) = \int_0^{l_0} \frac{1}{2} B(\kappa(t, g, a(g)) - \kappa_0(t))^2 J(t) dt + \int_0^{l_0} \frac{1}{2} EA(\lambda^2(t, g, a(g)) - 1)^2 J(t) dt \quad (28)$$

where  $J(t) := dS/dt = \sqrt{1 + X'_3{}^2}$ . The tip force  $f(g)$  being energy-conjugate to the tip displacement  $g$  is then given by

$$f(g) = \frac{d\widetilde{W}(g, a(g))}{dg} = \frac{\partial \widetilde{W}(g, a(g))}{\partial g} \bigg|_{a(g)} + \frac{\partial \widetilde{W}(g, a(g))}{\partial a} \frac{da(g)}{dg} \quad (29)$$

or

$$\begin{aligned} f(g) = & \int_0^{l_0} B(\kappa(t, g, a(g)) - \kappa_0(t)) \frac{\partial d\kappa(t, g, a(g))}{\partial dg} J(t) dt \\ & + \int_0^{l_0} EA(\lambda^2(t, g, a(g)) - 1) \frac{\partial d\lambda^2(t, g, a(g))}{\partial dg} J(t) dt. \end{aligned} \quad (30)$$

where, as previously, the fact that  $f$  and  $\widetilde{W}$  are functionals of  $\kappa$  and  $\lambda$  has been suppressed.

In order to complete the geometrical and constitutive description of the deforming sinusoidal elastica,  $s(g)$  must be obtained for each  $g$ . Apart from the main kinematic assumption that the deforming elastica maintains its sinusoidal shape, an additional constraint is required, as in the case of the elastica deforming as a circular arc. In the case of the sinusoidal elastica, the additional constraint determines the current amplitude  $a$ . As in Section 3 we consider the constraints of (i) inextensibility, (ii) an incompressible bounding medium, and (iii) stationary energy.

#### 4.1 Force-displacement response of an inextensible sinusoidal elastica

The local inextensibility condition requires that  $\lambda := ds/dS = 1$  and thus

$$\lambda^2 - 1 = \frac{1 + X'_3{}^2}{1 + X'_3{}^2} \frac{l^2}{l_0^2} - 1 = 0. \quad (31)$$

From (26) and (31) we have,

$$a^2 = a_0^2 - \frac{l^2 - l_0^2}{\pi^2 \cos^2(\alpha)}. \quad (32)$$

Clearly, the right hand-side of (32) can be negative, and is unbounded from below in the limit  $\alpha \rightarrow \pi/2$ . Even for positive values of the right hand-side, i.e.  $a^2 > 0$ ,  $a$  as given by (32) varies along the elastica. This indicates that the requirement that  $\lambda = 1$  pointwise along the elastica is inconsistent with maintenance of the sinusoidal shape. For this reason, we impose the inextensibility constraint over the half wavelength by enforcing conservation of the length of the sinusoidal elastica for a given tip displacement  $g$ . Additionally, we make the ansatz that  $a(g)$  is fixed over the half wavelength.

$$\int_s ds = \int_S dS \rightsquigarrow \int_0^{l_0} (\lambda(t, g, a) - 1) J(t) dt = 0. \quad (33)$$

This condition defines a non-linear residual that can be considered a function of  $a$ , which is itself dependent on  $g$ :

$$\mathcal{R}(a) := \int_0^{l_0} (\lambda(t, g, a) - 1) J(t) dt = 0 \quad (34)$$

In order to solve (34) a standard Newton-Raphson iterative scheme must be employed. Recall that this involves the linearization of the residual  $\mathcal{R}(a)$  about  $a = \bar{a}$ ,  $\text{Lin } \mathcal{R}(a)|_{\bar{a}} := \mathcal{R}(\bar{a}) + (\partial \mathcal{R} / \partial a)|_{\bar{a}} (a - \bar{a}) = 0$ , and the solution of this equation for  $a$  to get  $a = \bar{a} - \mathcal{R}(\bar{a}) / (\partial \mathcal{R} / \partial a)|_{\bar{a}}$ . For each given value of tip displacement  $g$ , this iterative update scheme is repeated until iterates for  $a$  converge to within a tolerance. Once the value of  $a$  is computed, we proceed with the computation of the tip force  $f$ . To this end, we need the sensitivity of the amplitude  $a(g)$  to the tip displacement  $g$ . It can be calculated by exploiting the implicit form of the residual, now written as  $\mathcal{R}(g, a(g))$  for a general displacement controlled loading process by writing  $d\mathcal{R}(g, a(g))/dg = (\partial \mathcal{R} / \partial g)|_a + (\partial \mathcal{R} / \partial a)(da/dg) = 0$  yielding  $da/dg = -(\partial \mathcal{R} / \partial g) / (\partial \mathcal{R} / \partial a)$ . With this sensitivity in hand, the integrands in (30) can be computed in a straightforward manner:

$$\begin{aligned} \frac{\partial d\kappa}{\partial dg} &= \frac{\partial \kappa}{\partial g} \Big|_a + \frac{\partial \kappa}{\partial a} \Big|_g \frac{da}{dg} = \frac{x_3''}{(1 + x_3'^2)^{5/2}} \left( \frac{(x_3'^2 - 2)}{l} + \frac{(1 - 2x_3'^2)}{a} \frac{da}{dg} \right), \\ \frac{\partial d\lambda^2}{\partial dg} &= \frac{\partial \lambda^2}{\partial g} \Big|_a + \frac{\partial \lambda^2}{\partial a} \Big|_g \frac{da}{dg} = \frac{2l}{l_0^2 (1 + X_3'^2)} \left( 1 + x_3'^2 \frac{l}{a} \frac{da}{dg} \right). \end{aligned} \quad (35)$$

## 4.2 Force-displacement response of a sinusoidal elastica surrounded by an incompressible medium

The incompressibility assumption on the surrounding medium (Figure 5) leads to an explicit, simple expression for the value of the current amplitude of the sinusoidal elastica  $a(g)$ .

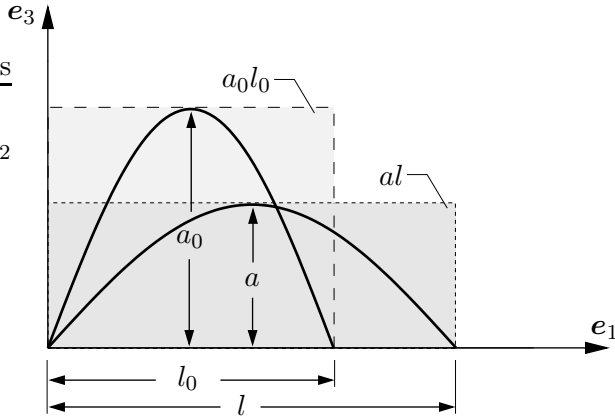


Figure 5: A sinusoidal elastica surrounded by an incompressible medium.

$$a_0 l_0 = a l \quad \rightsquigarrow \quad a(g) = \frac{a_0 l_0}{l} = \frac{a_0 l_0}{l_0 + g}. \quad (36)$$

Once  $a(g)$  is known explicitly in terms of tip displacement  $g$ , the derivatives appearing in (30) can be readily calculated

$$\frac{d\kappa}{dg} = \frac{3x_3''}{l} \frac{(x_3'^2 - 1)}{(1 + x_3'^2)^{5/2}} \quad \text{and} \quad \frac{d\lambda^2}{dg} = \frac{2l}{l_0^2} \frac{(1 - x_3'^2)}{(1 + X_3'^2)}. \quad (37)$$

### 4.3 Force-displacement response of a sinusoidal elastica with stationary energy

For the sinusoidal elastica, stationarity of energy is imposed with respect to the current amplitude  $a(g)$ , i.e.  $(\partial \widetilde{W}(g, a)/\partial a)|_g = 0$ . This condition defines a non-linear residual  $\mathcal{R}(a)$

$$\mathcal{R}(a) := \int_0^{l_0} \left( B(\kappa - \kappa_0) \frac{\partial \kappa}{\partial a} + EA(\lambda^2 - 1) \frac{\partial \lambda^2}{\partial a} \right) J(t) dt, \quad (38)$$

which must vanish for a given tip displacement  $g$ . As in Section (4.1) Equation (38) is solved for  $a$  by a Newton-Raphson iterative scheme.

With  $a$  being known the tip force,  $f$ , can be computed. Since the stationary energy condition requires that the partial derivative  $(\partial \widetilde{W}(g, a)/\partial a)|_g$  vanishes, the terms contributing to the force quantity will be only the partial derivatives of kinematic variables with respect to the tip displacement  $g$ . That is, it suffices to compute the integrand terms

$$\frac{\partial \kappa}{\partial g} = \frac{x_3''}{l} \frac{(x_3'^2 - 2)}{(1 + x_3'^2)^{5/2}} \quad \text{and} \quad \frac{\partial \lambda^2}{\partial g} = \frac{2l}{l_0^2} \frac{1}{(1 + X_3'^2)}. \quad (39)$$

**Remark 5:** Consider the limiting case in which the tip displacement  $g$  is much larger than the initial half-wavelength  $l_0$ , i.e.  $g/l_0 \gg 1$ , and  $l/l_0 \approx g/l_0 \gg 1$ . The elastica tends toward the limiting shape of a straight segment along  $e_1$ . Owing to the flat shape of the elastica, its spatial slope  $x_3'$  and the curvature  $x_3''$  are small. This implies that the contribution from the bending term to the overall tip force value in both (37)<sub>1</sub> and (39)<sub>1</sub> will be negligible in comparison with the contribution from the axial extension. Furthermore, the vanishing term  $x_3'$  in (37)<sub>2</sub> for large values of the tip displacement  $g$  makes the force terms in (37)<sub>2</sub> and (39)<sub>2</sub> tend toward each other. Then, provided the bending stiffness is not much larger than the axial stiffness, the tip force values for the incompressible bounding medium and stationary energy cases approach a common value at large tip displacement values. This is reflected in Figures 12 and 13.

**Remark 6:** Computations with all the models of the sinusoidal elastica discussed in the preceding Sections 4.1– 4.3 require an efficient numerical integration tool both for computing the tip force,  $f$ , and for carrying out the Newton-Raphson iterations. For this purpose, we have employed a set of F77 subroutines, the so-called DCUHRE, providing a double precision integration tool based on adaptive division of the integration domain into subregions. For details of the theory and the implementation of the algorithm, the reader is referred to Berntsen et al. (1991a; 1991b).

## 5 Comparison of kinematic and constraint assumptions; validation

We now turn to a comparative study and analysis of the force-displacement response of the circular and sinusoidal elasticas.

### 5.1 The force-displacement response of circular-arc and sinusoidal elasticas subjected to different constraint conditions

We first consider the force-stretch behavior of the circular-arc elastica subject to the three constraints. To this end, we make an assumption for the relation between the micro-tip displacement

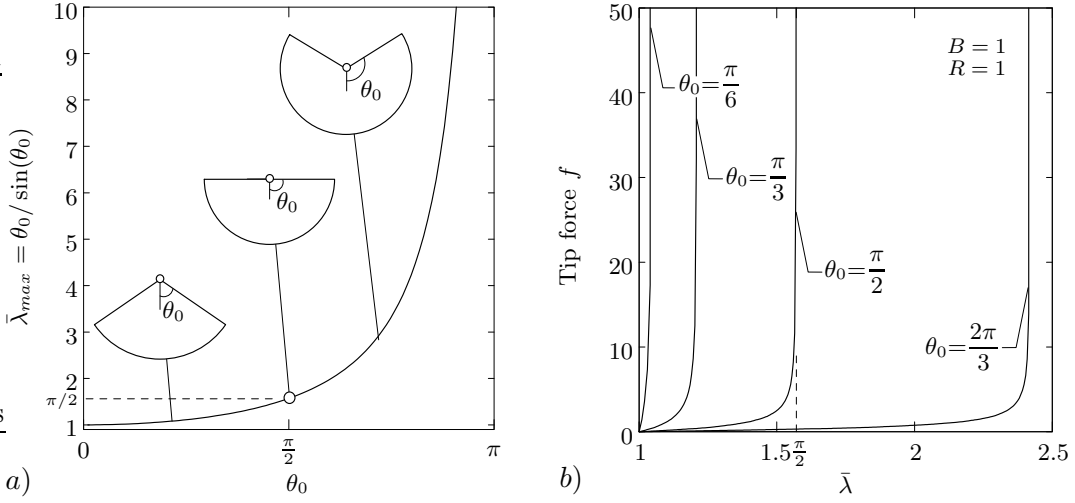


Figure 6: Circular-Arc inextensible elastica. a) Variation of the maximum macro-stretch  $\bar{\lambda}_{max} = \theta_0 / \sin(\theta_0)$  with the initial angle  $\theta_0$  for the circular-arc inextensible elastica. b) Shift of the maximum value of the attainable macro-stretch  $\bar{\lambda}_{max}$  for the selected values of the initial angle  $\theta_0 = \frac{\pi}{6}, \frac{\pi}{3}, \frac{\pi}{2}, \frac{2\pi}{3}$ .

$g$  and the macro-stretch  $\bar{\lambda}$ . The displacement between the ends of the elastica is assumed to be dictated by macroscopic deformation in an affine manner. That is, the macro-stretch  $\bar{\lambda}$  is related to the tip displacement  $g$  by  $\bar{\lambda} := 1 + g/(2R \sin(\theta_0))$  (see Figure 2). <sup>2</sup> In the subsequent analyses the macro stretch will be used as the primary deformation variable controlling the process.

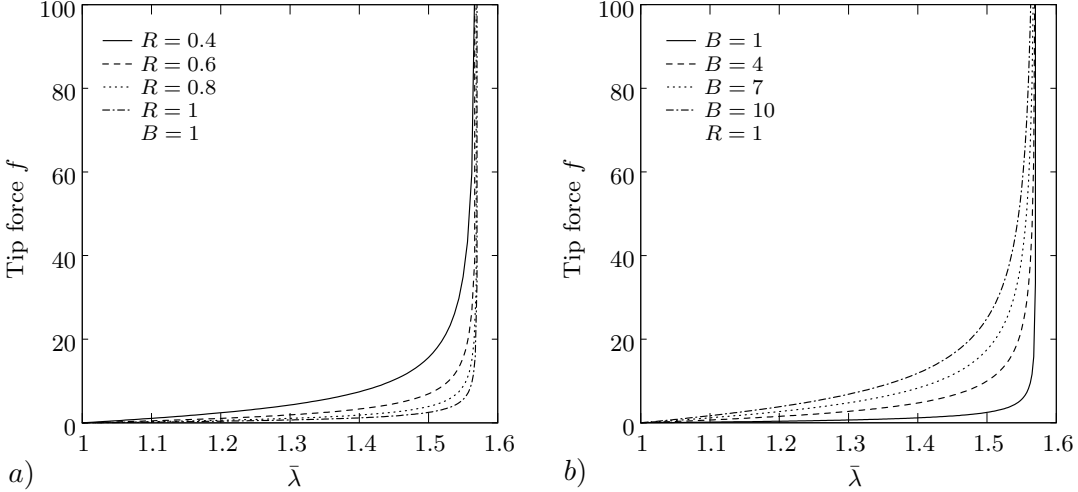


Figure 7: Circular-Arc inextensible elastica. Sensitivity analysis of the  $f-\bar{\lambda}$  curve to a) the variation of initial radius  $R \in [0.4, 1]$  and b) the variation of bending stiffness  $B \in [1, 10]$  for  $\theta_0 = \pi/2$ .

For the circular-arc, inextensible elastica, according to (12), the tip force  $f$  diverges as the tip displacement  $g$  approaches the value  $g_{max} = 2R(\theta_0 - \sin \theta_0)$ . This implies that the maximum value of macro-stretch is  $\bar{\lambda}_{max} = \theta_0 / \sin \theta_0$ , as shown also in Figures 6a and 6b. The geometric parameter  $\theta_0$  thus has an unambiguous physical effect. The ordinates of Figure 6a can be obtained as the locking stretch for each value of  $\theta_0$ . As shown more transparently in Figure 6b for the  $f-\bar{\lambda}$  response

<sup>2</sup>For tissues with transverse isotropy, where the collagen fibrils (elastica) are characterized by end-to-end vectors that are highly aligned, affinity of deformation is a good assumption. The alternative, fibril slippage, will be treated in a separate paper.

parametrized by  $\theta_0$ . For the circular-arc, inextensible elastica, the shape of the  $f-\bar{\lambda}$  curve depends only on the initial radius  $R$  and the bending stiffness  $B$ . Figures 7a and 7b demonstrate that the larger the initial radius  $R$  or the smaller the bending stiffness  $B$ , the sharper is the transition to the divergent behavior. Although the sharpness of the transition can be tuned, the value of the locking stretch is always fixed to the value  $\bar{\lambda}_{max} = \theta_0 / \sin \theta_0$  and the response beyond the heel region is asymptotic to a vertical line at  $\bar{\lambda}_{max}$ . Of course, this divergent  $f-\bar{\lambda}$  response is non-physical, and considerably limits the ability to match experiments on different collagenous materials possessing distinct, and non-divergent, responses in the post-heel region.

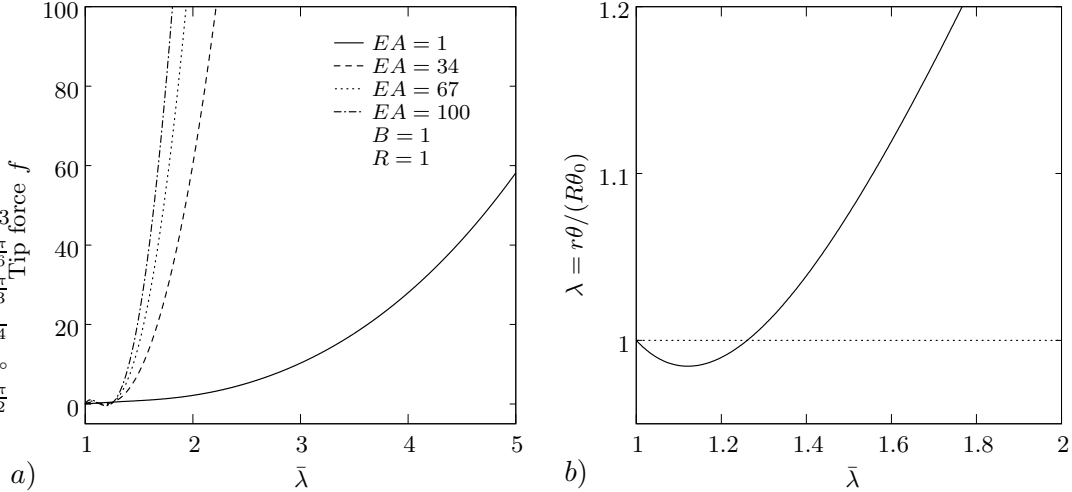


Figure 8: Circular-Arc elastica surrounded by an incompressible medium. a) Dependency of the micro-stretch  $\lambda$  on the macro-stretch  $\bar{\lambda}$  and the initial angle  $\theta_0$ . b) Sensitivity analysis of the  $f-\bar{\lambda}$  curve to the variation of the axial stiffness  $EA \in [1, 100]$ . curve.

The variation of the micro-stretch,  $\lambda$ , of a circular-arc elastica embedded in an incompressible medium for increasing macro-stretch,  $\bar{\lambda}$ , is depicted in Figure 8a. We draw attention in Figure 8b to the compression of the elastica for a regime of deformation characterized by small values of  $\bar{\lambda}$ , and discussed in Remark 3. Following the approach outline there we have solved for  $\theta_0 = \theta_{0,cr}$  such that for all  $\theta_0 < \theta_{0,cr}$  we have  $d\lambda/d\bar{\lambda} > 0$ . Explicitly we have  $\lambda = \theta(\bar{\lambda})r(\bar{\lambda})/(R\theta_0)$  with  $r(\bar{\lambda}) = R(1 - \cos(\theta_0))/(2\bar{\lambda}) + \bar{\lambda}^3 R \sin^2(\theta_0)/(2(1 - \cos(\theta_0)))$  and  $\theta(\bar{\lambda}) = \sin^{-1}(\bar{\lambda}R \sin(\theta_0)/(r\bar{\lambda}))$ . Setting the derivative  $d\lambda/d\bar{\lambda}|_{\bar{\lambda}=1} = 0$  and solving the resulting equation for  $\theta_0$ , we obtained the upper bound  $\theta_0 \leq \theta_{0,cr} \approx 1.342$ . As clearly shown in Figure 8a, for the values of the initial angle  $\theta_0 \leq \theta_{0,cr}$  the compressive regime of macro-stretch values is avoided. For this reason our subsequent investigations are restricted to the range  $\theta_0 \leq \theta_{0,cr}$  for the circular-arc elastica embedded in an incompressible medium.

The sensitivity of the tip force,  $f$ , to the axial stiffness,  $EA$ , for  $B = 1$ ,  $R = 1$  and  $\theta_0 = \pi/3$  is depicted in Figure 8a for the circular-arc elastica surrounded by an incompressible medium. A decrease in the axial stiffness translates, as expected, to a decrease of the slope. Clearly, the axial stiffness dominates the stiffness of the  $f-\bar{\lambda}$  curve. In contrast to the inextensible case we observe neither a long toe region nor a distinguishable heel region. Larger values of  $\bar{\lambda}$  are attainable. As the axial stiffness is increased, however, the  $f-\bar{\lambda}$  curve starts to get asymptotic about  $\bar{\lambda}_{max} = \theta_0 / \sin \theta_0$  without exhibiting much of a toe region. This, of course, limits the use of this model.

The last case for the circular-arc geometry is concerned with stationarity of energy. The material parameters used were the same as for the incompressible medium. As in the incompressible case a decrease in axial stiffness has a strong, depressing influence on stiffness of the  $f-\bar{\lambda}$  response.

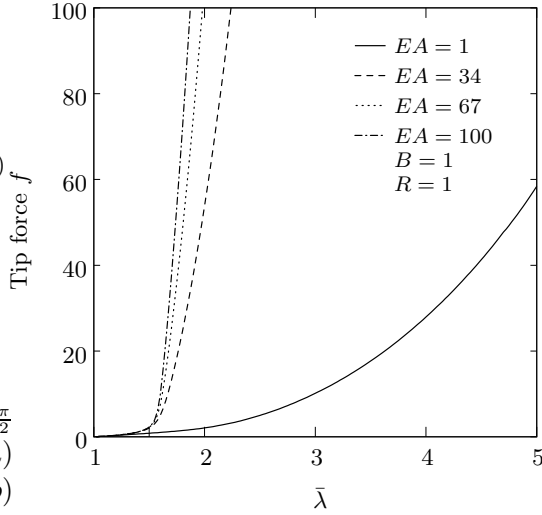


Figure 9: Circular-arc elastica with stationary energy. Sensitivity analysis of the  $f - \bar{\lambda}$  curve to the variation of the axial stiffness  $EA \in [1, 100]$ .

The elastica can be extended to  $\bar{\lambda} > \theta_0 / \sin \theta_0$ . With an increase in axial stiffness, the  $f - \bar{\lambda}$  curve approaches the behavior of the inextensible circular-arc elastica (see Figure 9). The circular-arc elastica finding its form by attaining a stationary state of energy possesses a number of favorable properties: The toe region exists and its slope can be tuned by the bending stiffness. The location of the heel region is uniquely determined by the initial angle  $\theta_0$ . The slope of the post-heel region can be adjusted by the axial stiffness  $EA$  as shown in Figure 9. The stationary energy assumption with clearly identifiable parameters thus serves as a promising model for fitting of experimental data.

In Figure 10 we compare all three cases of the circular-arc elastica. Distinct values  $EA = 34, 67, 100$  are assigned to the axial modulus of the incompressible and stationary energy elasticas. The  $f - \bar{\lambda}$  curve of the stationary energy case approaches the inextensible one by “rotating” about the heel just below  $\bar{\lambda}_{\max}$ . However, this occurs with no discernible difference in the curves for  $\lambda$  values smaller than the heel. In case of the elastica surrounded by an incompressible medium, however, the stiffening in the  $f - \bar{\lambda}$  behavior is different. Owing to the small values of micro-stretch in the initial stages, the location of the heel is shifted to smaller values of  $\bar{\lambda}$ .

In the foregoing parameter study, we solely considered circular-arc elasticas with the three constraints on deformation. In what follows, we present an analogous parameter sensitivity study for the sinusoidal geometry. In contrast to the circular-arc elastica, the reference shape of a sinusoidal elastica is governed by two parameters: the amplitude  $a_0$  and the half-wave length  $l_0$  (see Figure 4). The order of the ratio of the amplitude to the half-wave length  $a_0/l_0$ , however, cannot be arbitrarily chosen. According to the results reported by Dale et al. (1972), this ratio is limited to values smaller than 0.1. Taking into account this fact in the subsequent analyses, the value of this ratio will be chosen to be  $a_0/l_0 < 0.2$ , which will allow us to consider values slightly larger than the experimental observations. Furthermore, analogous to the study on the circular-arc elasticas, the macro-stretch  $\bar{\lambda}$  will be considered as the primary deformation measure which is related to the tip displacement  $g$  by  $\bar{\lambda} := 1 + g/l_0$ .

First, we consider a sinusoidal elastica that is constrained to the global inextensibility condition given in (33). In Figure 11a the influence of the ratio  $a_0/l_0$  on the  $f - \bar{\lambda}$  curve is depicted. The value of  $a_0/l_0$  is increased from 0.05 to 0.2 while keeping the values of the material parameters

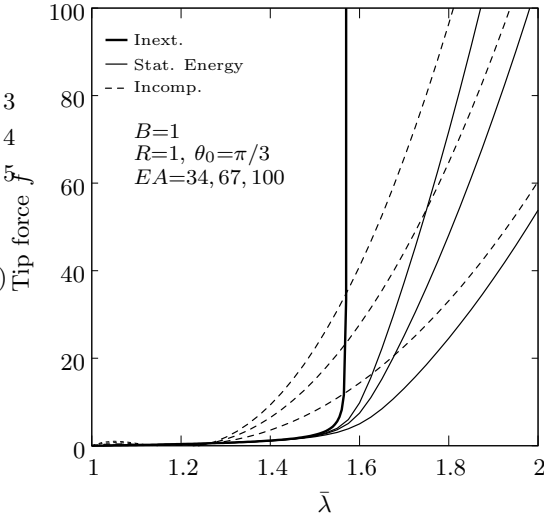


Figure 10: Comparison of circular-arc elasticas subjected to different constraints. In the incompressible and stationary energy cases, three different values are assigned to the axial modulus  $EA = 34, 67, 100$ .

fixed at  $B = 1$  and  $EA = 1$ . This ratio proves crucial in determining the value of stretch at which the heel occurs. The higher the ratio  $a_0/l_0$ , the longer the toe region preceding the heel. In other words, this parameter determines the value of  $\bar{\lambda}$  where the influence of the bending mechanism starts to diminish and the axial extension begins to govern the  $f-\bar{\lambda}$  curve. In order to demonstrate the sensitivity of the  $f-\bar{\lambda}$  curve to the bending stiffness, the ratio of bending stiffness to axial stiffness,  $B/EA$ , is varied from 1 to 4 (Figure 11b). An increase in the ratio  $B/EA$  scales the curve's ordinates ( $f$ -values), and therefore the transition in the heel region becomes more gradual. However, the value of the locking stretch is not influenced by the changes in the ratio  $B/EA$ .

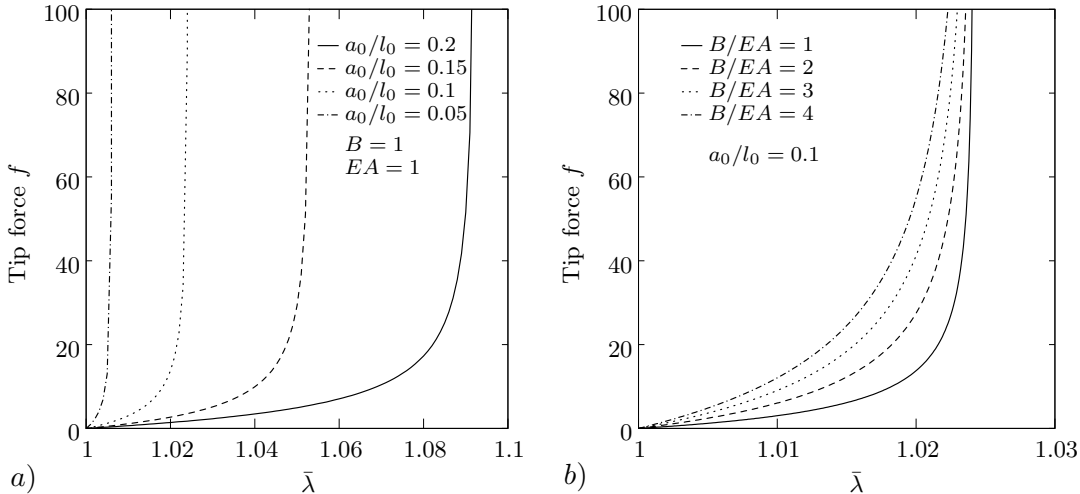


Figure 11: Sinusoidal inextensible elastica. Comparison of the  $f-\bar{\lambda}$  curves for globally inextensible sinusoidal elasticas having different a)  $a_0/l_0$  and b)  $B/EA$  ratios.

In the last two cases we consider the incompressible and stationary energy sinusoidal elasticas. Figures 12a and 13a present the influence of the change in ratio  $a_0/l_0$  on the  $f-\bar{\lambda}$  curves of the respective cases. Like the inextensible case the ratio  $a_0/l_0$  is varied within the interval  $[0.05, 0.2]$

while the value of the ratio  $EA/B$  is kept fixed at 30. Clearly, the  $f-\bar{\lambda}$  curves for the incompressible and stationary energy cases do not exhibit a pronounced stiffening behavior. This is in contrast with the inextensible case, see Figure 11. Variation of the ratio  $a_0/l_0$  does not cause significant change in the shape of the curves.

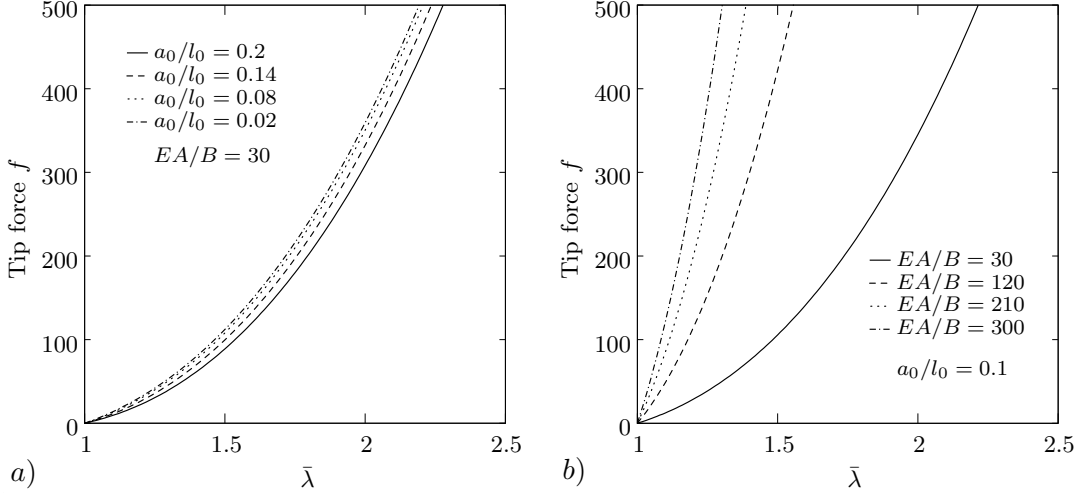


Figure 12: Sinusoidal elastica surrounded by an incompressible medium. Comparison of the  $f-\bar{\lambda}$  curves for different a)  $a_0/l_0$  and b)  $EA/B$  ratios.

The sensitivity of the  $f-\bar{\lambda}$  curves for the separate cases to changes in material parameters  $EA$  and  $B$  is presented in Figures 12b and 13b, respectively. The ratio  $EA/B$  varies in the range  $[30, 300]$ . The axial stiffening is clearly reflected in the curves. No striking shape change is observed. It should be noticed that the  $f-\bar{\lambda}$  curves in Figures 12 and 13 for the incompressible and stationary energy cases of the sinusoidal elastica are quite similar. The reasons for this similarity have been already outlined in Remark 5.

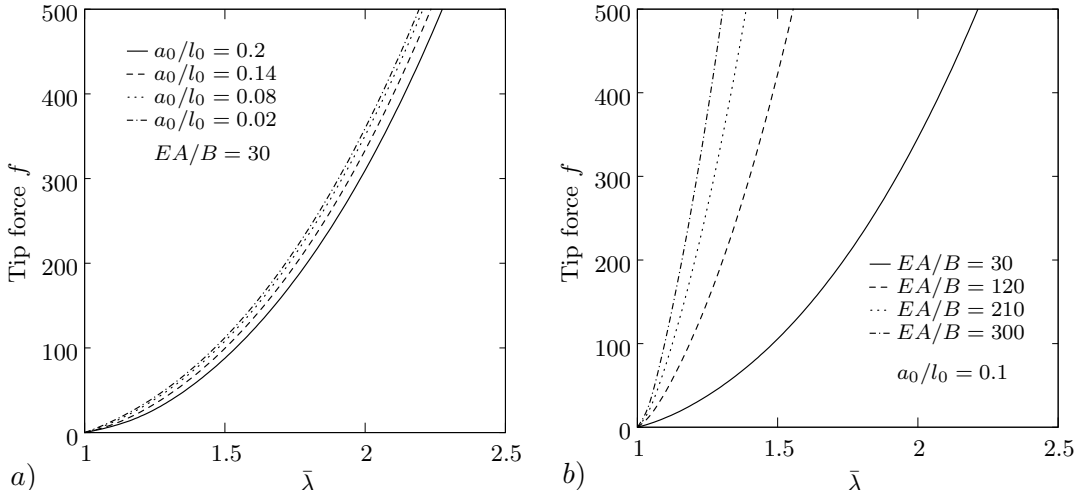


Figure 13: Sinusoidal elastica deforming by attaining a stationary energy state. Comparison of the  $f-\bar{\lambda}$  curves for different a)  $a_0/l_0$  and b)  $EA/B$  ratios.

## 5.2 Validation of constraint assumptions by numerical simulations

In the preceding section the sensitivities of the  $f - \bar{\lambda}$  curves to geometric and material parameters have been discussed for both the circular-arc and the sinusoidal elastica subjected to the three constraint conditions. In this section we carry out a comparison with data recently reported by Freed and Doehring (2005) (Figure 14). These data acquired correspond to uniaxial extension

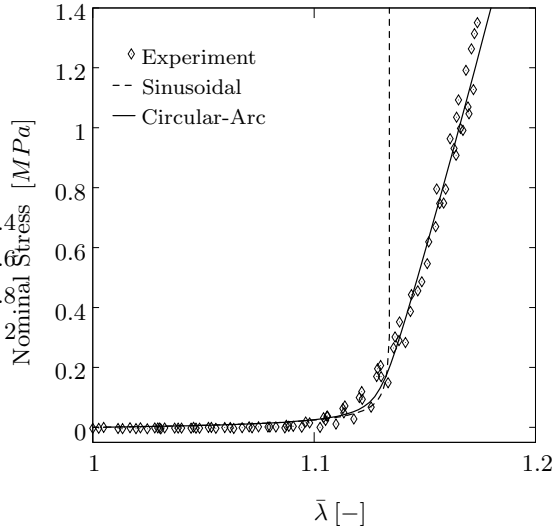


Figure 14: Simulations of experimental data by the inextensible sinusoidal elastica ( $a_0/l_0 = 0.245$ ,  $B/EA = 25 \text{ mm}^{-1}$ ) and the circular-arc elastica attaining a stationary energy state ( $R = 0.013 \text{ mm}$ ,  $\theta_0 = 4\pi/15 (= 48^\circ)$ ,  $EA/B = 7 \cdot 10^6 \text{ mm}^{-2}$ ). In the calculations  $r_0, a_0$  and  $l_0$  were in  $\text{mm}$   $B$  in  $\text{N/mm}$  and  $EA$  in  $\text{MPa/mm}$ .

experiments on five chordae tendineae from porcine mitral valves. They demonstrate a long toe region relative to the maximum stretch in each experiment. Beyond the heel region ( $\bar{\lambda} \approx 1.13$ ), the nominal stress–stretch curve is almost linear with a sharply larger slope. From the results in Figures 6-13 of the preceding parameter study, it is apparent that this behavior can only be captured either by the inextensible sinusoidal elastica, or the circular-arc elastica attaining a stationary energy state. Figure 14 compares the experiment with these two models with the material parameters given in the caption. Both the sinusoidal and the circular-arc model successfully match the data in the toe region. The inextensible sinusoidal model can also predict the upturning region, but its stiffness beyond the heel region rapidly diverges and fails to match the experimental results. In the case of the circular-arc model, the value of  $\theta_0$  can be analytically determined by assigning the macro-stretch value of the heel region ( $\bar{\lambda} \approx 1.13$ ) to the limiting case where we look for  $\theta_0$  such that  $\theta_0/\sin \theta_0 = \bar{\lambda}_{\text{heel}} = 1.13$ . Once the initial angle  $\theta_0 = 2\pi/7.5$  is computed the ratio of the axial and bending stiffness  $EA/B$  can be tuned to match the slopes of the regions just preceding and succeeding the heel region. The initial radius  $R$  is varied to match the sharpness of the slope change at the heel region. The comparison of the stationary energy circular-arc elastica and the experimental data clearly illustrates that the proposed model quantitatively captures the experimental data with just a few parameters:  $\theta_0, R, B$  and  $EA$ , all of which are very well-motivated physically.

## 6 Macroscopic material model incorporating the elastica

### 6.1 Continuum strain energy functions at the macroscale

The contribution to the overall strain energy function per unit reference volume due to the collagen fibrils embedded in a nearly incompressible viscous medium is obtained by summing up the free energies of individual elasticas

$$\Psi_{\text{col}} = \frac{N}{A_0 l_0} \widetilde{W}(g) . \quad (40)$$

With the unit vector  $\mathbf{e}$  denoting the average orientation of collagen fibrils, the macroscopic stretch in this direction is obtained by  $\bar{\lambda} = |\mathbf{F}\mathbf{e}|$ , where  $\mathbf{F}$  is the deformation gradient tensor. In the context of anisotropic elasticity, especially transverse isotropy, it is common to define structural tensors  $\mathbf{M} := \mathbf{e} \otimes \mathbf{e}$  for the construction of strain energy functions formulated in terms of additional invariants. The derivatives of these invariants are then used as tensor generators in the stress response functions. In the present case,  $I_4 := \mathbf{C} : \mathbf{M} = \bar{\lambda}^2$  is the relevant invariant ( $\mathbf{C}$  being the right Cauchy-Green tensor). We continue to use an affine relation between the macro-stretch and tip displacement of fibrils, i.e.  $\bar{\lambda} = (l_0 + g)/l_0$ . With this relation in hand, the contribution to the total second Piola-Kirchhoff stress tensor due to the stretching of collagen fibers  $\mathbf{S}^{\text{col}} = 2\partial\Psi_{\text{col}}/\partial\mathbf{C}$  can be obtained as

$$\mathbf{S}^{\text{col}} = N \frac{f(g)/\bar{\lambda}}{A_0} \mathbf{M} \quad (41)$$

where the results  $\partial g/\partial\bar{\lambda} = l_0$ ,  $2\partial\bar{\lambda}/\partial I_4 = 1/\bar{\lambda}$ ,  $\partial I_4/\partial\mathbf{C} = \mathbf{M}$  and the definition  $f(g) := d\widetilde{W}/dg$  have been used. Then, the nominal stress tensor  $\mathbf{P}^{\text{col}}$  readily follows  $\mathbf{P}^{\text{col}} = \mathbf{F}\mathbf{S}$

$$\mathbf{P}^{\text{col}} = N \frac{f(g)}{A_0} \tilde{\mathbf{e}} \otimes \mathbf{e} \quad (42)$$

where  $\mathbf{F}\mathbf{e} = \bar{\lambda}\tilde{\mathbf{e}}$  and  $|\tilde{\mathbf{e}}| = 1$ .

We now turn attention to the convexity of the strain energy  $\Psi_{\text{col}} = \hat{\Psi}_{\text{col}}(I_4)$ , in order to have a basic understanding of its stability properties. The convexity condition demands the positive definiteness of the first elasticity tensor  $\mathbb{A}^{\text{col}}$

$$\mathbf{H} : \mathbb{A}^{\text{col}} : \mathbf{H} \geq 0 \quad \forall \mathbf{H} \in \mathbb{M}^{3 \times 3} \quad \text{and} \quad \mathbb{A}^{\text{col}} := \frac{\partial^2 \hat{\Psi}_{\text{col}}}{\partial \mathbf{F} \partial \mathbf{F}} . \quad (43)$$

where  $\mathbb{M}^{3 \times 3}$  is the space of second-order tensors in  $\mathbb{R}^3$ .

The explicit form of the first elasticity tensor  $\mathbb{A}^{\text{col}}$  can be obtained through chain rule operations as

$$\mathbb{A}^{\text{col}} := \hat{\Psi}'_{\text{col}} \frac{\partial^2 I_4}{\partial \mathbf{F} \partial \mathbf{F}} + \hat{\Psi}''_{\text{col}} \frac{\partial I_4}{\partial \mathbf{F}} \otimes \frac{\partial I_4}{\partial \mathbf{F}} . \quad (44)$$

Forming the quadratic product of  $\mathbb{A}^{\text{col}}$  with  $\mathbf{H}$  involves the terms

$$\mathbf{H} : \frac{\partial^2 I_4}{\partial \mathbf{F} \partial \mathbf{F}} : \mathbf{H} = 2\|\mathbf{H}\mathbf{e}\|^2 \geq 0 , \quad \left( \frac{\partial I_4}{\partial \mathbf{F}} : \mathbf{H} \right)^2 = (2\mathbf{H}\mathbf{e} \cdot \mathbf{F}\mathbf{e})^2 \geq 0 . \quad (45)$$

Note that both terms are non-negative. The local convexity condition (43) of the free energy  $\hat{\Psi}_{\text{col}}$  reduces to

$$2\hat{\Psi}'_{\text{col}} |\mathbf{H}\mathbf{e}|^2 + 4\hat{\Psi}''_{\text{col}} (\mathbf{H}\mathbf{e} \cdot \mathbf{F}\mathbf{e})^2 \geq 0 . \quad (46)$$

Based on (45), non-negativity of both  $\hat{\Psi}'_{\text{col}}$  and  $\hat{\Psi}''_{\text{col}}$  is sufficient to fulfill the convexity condition (46), though not necessary. The explicit forms of the derivatives are  $\hat{\Psi}'_{\text{col}} = Nf(g)/(2A_0\bar{\lambda})$  and  $\hat{\Psi}''_{\text{col}} = Nl_0(f'(g)l_0 + gf'(g) - f(g))/(4A_0\bar{\lambda}^2(g + l_0))$ . If we assume that collagen fibrils can carry only tensile loads, i.e. tension only elasticas, the positiveness of  $\hat{\Psi}'_{\text{col}}$  is satisfied identically for  $f(g) \geq 0$ . Furthermore, the convexity of  $\hat{\Psi}_{\text{col}}$  with respect to  $g$  ensures that  $f'(g) \geq 0$ . Thus, it is now sufficient to show that the term  $gf'(g) - f(g) \geq 0$  in  $\hat{\Psi}''_{\text{col}}$ . This condition can be obtained starting from the convexity condition for  $f(g)$  with respect to  $g$ , i.e.  $f''(g) \geq 0$ . For positive values of  $g$ , we have  $gf''(g) \geq 0$ . Integration of  $gf''(g) \geq 0$  by parts yields  $\int_0^g gf''(g) = gf'(g)|_0^g - \int_0^g f'(g) \geq 0$ . For  $f(0) = 0$ , we obtain the sought form  $gf'(g) - f(g) \geq 0$ . Therefore, convexity of both the  $\widetilde{W}$  and  $f(g) = d\widetilde{W}/dg$  guarantees the local convexity of the macroscopic free energy function  $\hat{\Psi}_{\text{col}}$ .

When  $\hat{\Psi}_{\text{col}}$  is combined by rule-of-mixtures with the strain energy density function of the surrounding matrix medium, the above results completely characterize the influence upon the convexity of the overall composite, leaving open only the question of convexity of the matrix material.

## 7 Closing remarks

The primary aim of this paper is a discussion of the characteristic soft tissue response in the context of the elastica-like response of slender fibrillar structures in these tissues. The models are applicable to tendons, skin and the passive response of muscle. While entropic elasticity-based models can also model the this characteristic soft tissue response—especially the locking behavior—there are strong physical and physiological reasons to surmise that this is the wrong approach to adopt. A direct solution of the shape, and force in a deforming elastica requires the solution of a (“highly”) nonlinear, fourth-order partial differential equation. The simplification used here is that judiciously-chosen constraints, on the kinematics and on the energy state, can lead to force-deformation response functions for the elastica. This is the central thesis advanced in this paper. Beyond this, the paper is concerned with an enumeration of two families of shapes (circular arcs and sinusoidal half-periods) of the deforming elastica, and three possible additional constraints. These additional constraints: inextensibility, macroscopic incompressibility, and stationarity of energy are well-founded in a physical sense. Their suitability in matching a set of experimental force-deformation curves has been examined. On the basis of the current limitation to elastic effects, it emerges that the elastica deforming as a circular arc, and maintaining itself in a state of stationary energy in each configuration (parametrized by overall elongation) can resolve the experimental data to an arbitrary degree of precision.<sup>3</sup> The parameters use are two the stiffness—bending and axial, and two geometric parameters that determine the shape of the undeformed elastica. These can be easily determined from mechanical experiments and micrographs, and compared with the values obtained for the best fit. Such an exercise would be a strong validation of these models. We note that the circular-arc elastica with stationary energy matches the experimental data very well in Figure 14 with initial radius  $R = 0.013$  mm (13  $\mu\text{m}$ ), and initial central angle  $2\theta_0 = 8\pi/15$  ( $96^\circ$ ). This gives a wavelength of  $2R \sin \theta_0 = 38.64 \mu\text{m}$  which seems very reasonable, given that collagen fibrils are typically found to have wavelengths between 10 and 50  $\mu\text{m}$  as in Screen et al. (2003); Provenzano and Vanderby (2006). The importance of inelastic effects such as the viscous friction as collagen fibrils move relative to the surrounding proteoglycans, viscoelasticity of the proteoglycans themselves, and slippage of fibrils under larger forces, must not be overlooked, however.

---

<sup>3</sup>We we have not demonstrated quantitative error measures since no significant physical insight is gained by doing so.

It should also be quite clear, that the development here has complete relevance for any slender filamentous structure, from carbon nanotubes, through underwater cables to oil pipelines. The class of continuum strain energy density functions so developed in Section 6 is applicable to any composite consisting of mainly unidirectional, elastica-like reinforcing fibers in a matrix.

## References

Basu, A. J., Lardner, T. J., 1985. Deformation of a planar sinusoidal elastic beam. *Journal of Applied Mathematics and Physics* 36, 460–474.

Berntsen, J., Espelid, T. O., Genz, A., 1991a. An adaptive algorithm for the approximate calculation of multiple integrals. *ACM Transactions on Mathematical Software* 17 (4), 437–451.

Berntsen, J., Espelid, T. O., Genz, A., 1991b. Algorithm 698: Dcuhre: An adaptive multidimensional integration routine for a vector of integrals. *ACM Transactions on Mathematical Software* 17 (4), 452–456.

Beskos, D. E., Jenkins, J. T., 1975. A mechanical model for mammalian tendon. *jam* 42, 755–758.

Buckley, C. P., Lloyd, D. W., Konopasek, M., 1980. On the deformation of slender filaments with planar crimp: theory, numerical solution and applications to tendon collagen and textile materials. *prsla* 372, 33–64.

Comninou, M., Yannas, I. V., 1976. Dependence of stress-strain nonlinearity of connective tissues on the geometry of collagen fibers. *jbm* 9, 427–433.

Dale, W. C., Baer, E., Keller, A., Kohn, R. R., 1972. On the ultrastructure of mammalian tendon. *Experientia* 28, 1293–1295.

Diamant, J., Keller, A., Baer, E., Litt, M., Arridge, R. G. C., 1972. Collagen; ultrastructure and its relation to mechanical properties as a function of ageing. *prslb* 180, 293–315.

Freed, A. D., Doehring, T. C., 2005. Elastic model for crimped collagen fibrils. *ASME Journal of Biomechanical Engineering* 127, 587–593.

Fung, Y. C., 1993. *Biomechanics: Mechanical Properties of Living Tissues*. Springer-Verlag.

Hurschler, C., LoitzRamage, B., Vanderby, R., 1997. A structurally-based stress-stretch relationship for tendon and ligament. *jbme* 119, 392–399.

Kastelic, J., Palley, J., Baer, E., 1980. A structural mechanical model for tendon crimping. *jbm* 13, 887–893.

Kratky, O., Porod, G., 1949. Röntgenuntersuchungen gelöster Fadenmoleküle. *Recueil Trav. Chim* 68, 1106–1122.

Landau, L. D., Lifshitz, E. M., 1951. *A Course on Theoretical Physics, Volume 5, Statistical Physics, Part I*. Butterworth Heinemann (reprint).

Lanir, Y., 1978. Structure-strength relations in mammalian tendon. *Biophys. J.* 24, 541–554.

Ogden, R. W., 1997. *Nonlinear Elastic Deformations*. Dover Publications, Mineola, N.Y.

Provenzano, P. P., Vanderby, R., 2006. Collagen fibril morphology and organization: Implications for force transmission in ligament and tendon. *Matrix Biology* 25, 71.

Screen, H. R. C., Lee, D. A., Bader, D. L., Shelton, J. C., 2003. An investigation into the effects of the hierarchical structure of tendon fascicles on micromechanical properties. *Proc. Instn. Mech. Engr* 218, 109.

Stouffer, D. C., Butler, D. L., Hosny, D., 1985. The relationship between crimp pattern and mechanical response of human patellar tendon-bone. *jbme* 107, 158–165.

Sun, Y.-L., Luo, Z.-P., Fertala, A., An, K.-N., 2002. Direct quantification of the flexibility of type I collagen monomer. *Biochemical and Biophysical Research Communications* 4295, 382–386.

Treloar, L. R. G., 1975. *The physics of rubber elasticity*. Oxford Clarendon Press.

Woo, S. L.-Y., Lee, T. Q., Gomez, M. A., Sato, S., Field, F. P., 1987. Temperature-dependent behavior of the canine medial collateral ligament. *J. Bio. Mech. Engrg. Trans ASME* 109, 68.